SUPPORTING INFORMATION

Iron-Sequestering Nanocompartments as Multiplexed Electron Microscopy Gene Reporters

Felix Sigmund,[†,‡,§,¶] Susanne Pettinger,[†,‡,§,¶] Massimo Kube,[||,¶] Fabian Schneider,[||] Martina Schifferer,[⊥,#] Steffen Schneider,[⊗,▽] Maria V. Efremova,[†,‡,§,^] Jesús Pujol-Martí,[&] Michaela Aichler,[○] Axel Walch,[○] Thomas Misgeld,[⊥,#] Hendrik Dietz,[||] Gil G. Westmeyer*[,†,‡,§]

[†]Department of Nuclear Medicine, TUM School of Medicine, Technical University of Munich, 81675 Munich, Germany
[‡]Institute of Biological and Medical Imaging, Helmholtz Zentrum München, 85764 Neuherberg, Germany
[§]Institute of Developmental Genetics, Helmholtz Zentrum München, 85764 Neuherberg, Germany
[||]Laboratory for Biomolecular Design, Department of Physics, Technical University of Munich, 85748 Garching, Germany
[⊥]Institute of Neuronal Cell Biology, TUM School of Medicine, Technical University of Munich, 80802 Munich, Germany
[#]German Center for Neurodegenerative Diseases (DZNE), 81377 Munich, Germany
[⊗]Computational Neuroengineering, Department of Electrical and Computer Engineering, Technical University of Munich, 80333 Munich, Germany
[▽]Tübingen AI Center, University of Tübingen, 72076 Tübingen, Germany
[^]Laboratory of Chemical Design of Bionanomaterials for Medical Applications, Department of Chemistry, Lomonosov Moscow State University, 119991 Moscow, Russian Federation
[&]Department “Circuits - Computation - Models”, Max Planck Institute of Neurobiology, 82152 Martinsried, Germany
[○]Research Unit Analytical Pathology, Helmholtz Zentrum München, 85764 Neuherberg, Germany

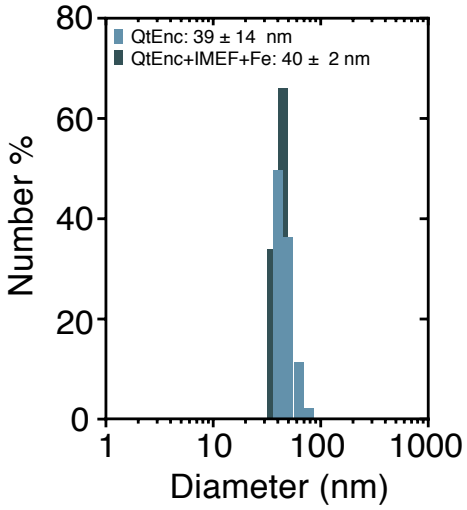

Supplementary Figure 1. DLS measurement of purified encapsulin nanospheres. Dynamic light scattering (DLS) measurements of purified QtEnc without or with QtIMEF and iron loading purified from HEK293T cells. The histogram shows monodisperse distributions for both samples.

¶ contributed equally
* corresponding author

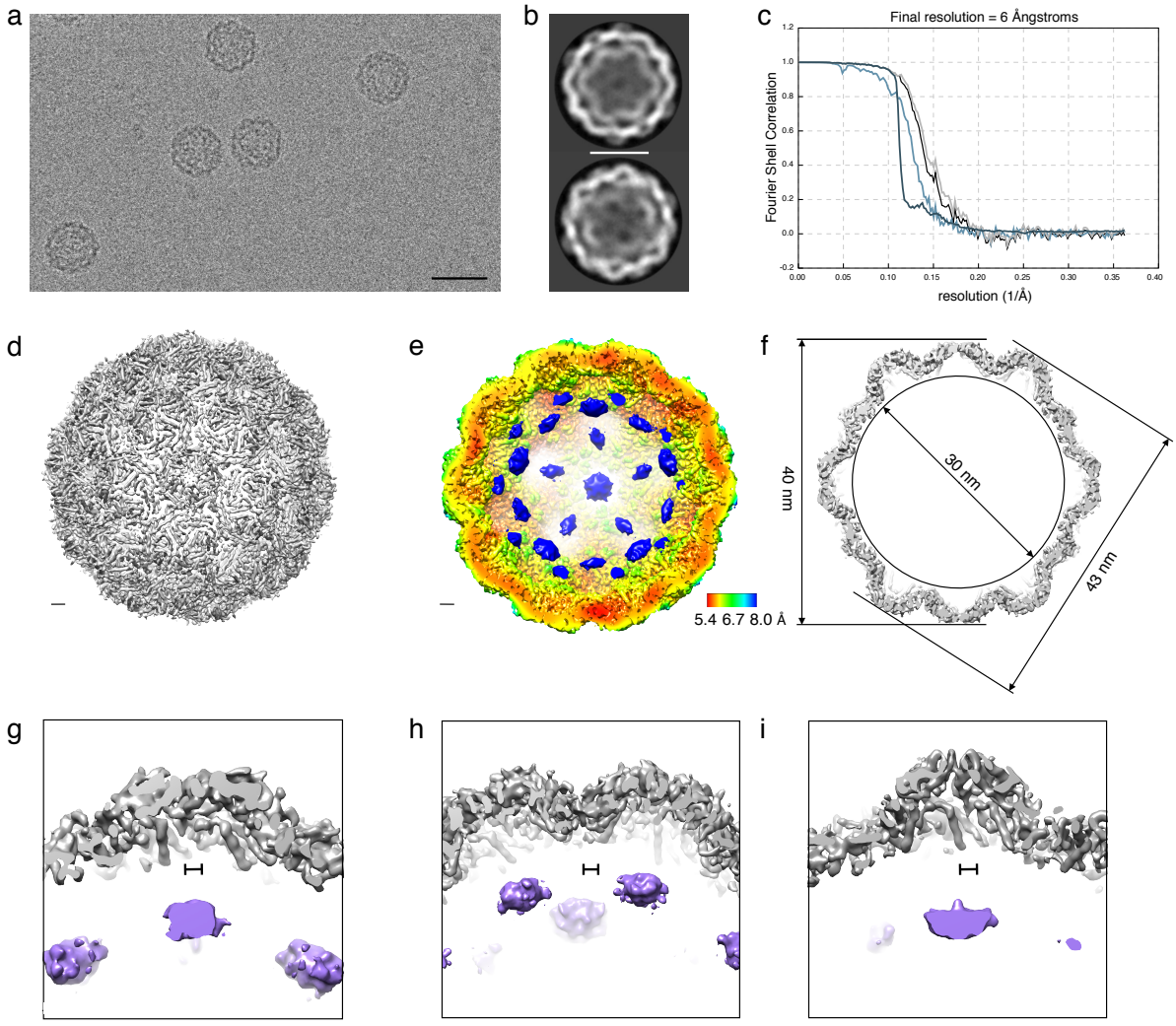

Supplementary Figure 2. Cryo-EM of QtEnc+QtIMEF purified from HEK293E cells. (a) Exemplary micrograph of QtEnc nanospheres co-expressing QtIMEF cargo purified from mammalian cells. The scale bar represents 50 nm. **(b)** Exemplary 2D class averages of QtEnc+QtIMEF; scale bar is 25 nm. **(c)** Fourier shell correlation (FSC) curves of the final post-processed map showing the FSC of unmasked (light turquoise) and masked (light grey) maps as well as the corrected curve (black) of phase randomized, masked maps (dark turquoise). **(d)** Electrostatic potential map of QtEnc+QtIMEF; scale bar represents 2 nm. **(e)** Cutaway view of the QtEnc shell color-coded by local resolution; QtIMEF is shown in blue. Scale bar is 2 nm. **(f)** Inner and outer diameters (through two-fold and five-fold axes) shown on a slice representation through the center of QtEnc. **(g)** Close-up through the five-fold symmetry of the QtEnc shell (grey) with an ~1 nm-sized pore. QtIMEF density (purple) is located at an ~2.5 nm distance to the pore. **(h)** Zoomed-in view through the three-fold symmetry center with a putative pore region in its center. **(i)** Zoom-in to the two-fold symmetry center. The ~1 nm sized cleft appears to be closed by two touching QtEnc monomers. QtIMEF density (purple) can be found ~2.5 nm below the cleft. Scale bars in g,h,i represent 1 nm.

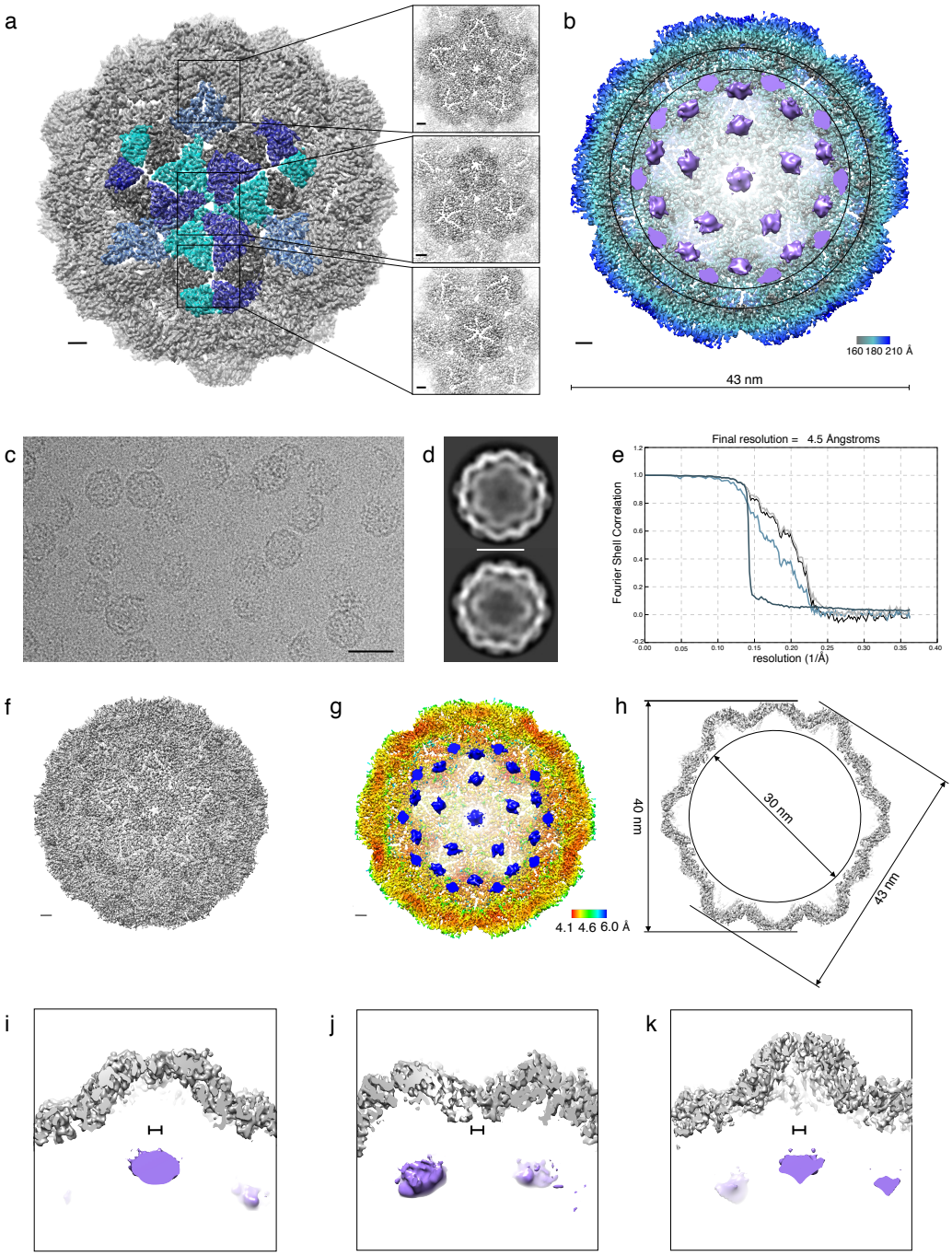

Supplementary Figure 3. Cryo-EM of QtEnc+QtIMEF purified from *E.coli*. (a) Segmented electron density of QtEnc co-expressed with QtIMEF cargo purified from *E.coli*. The four different monomer conformations are colored according to their interconnectivity and position. The five-fold centers are on opposite sides of a three-fold center with two monomers in between, which indicates a $T = 4$ icosahedral symmetry of the shell. Boxes show zoomed-in views of the five-fold, three-fold, and two-fold symmetry centers. The resolution of the map is 4.5 Å; scale bars represent 2 nm. **(b)** Cutaway view through the maximum diameter of QtEnc (43 nm) co-expressed with QtIMEF cargo. The shell is radially color-coded for local resolution, and QtIMEF cargo is shown in violet at different electron densities. A gap of ~2.5 nm is apparent between cargo and shell. **(c)** Exemplary micrograph of QtEnc nanocompartments co-expressing QtIMEF purified from *E.coli*. Scale bar represents 50 nm. **(d)** Exemplary 2D class averages of QtEnc; scale bar is 25 nm. **(e)** FSC curves of the final post-processed map showing the Fourier shell correlations of unmasked (light turquoise) and masked (light grey) maps as well as the corrected curve (black) and the corrected curve of phase randomized, masked maps (dark turquoise). **(f)** Electrostatic potential map of QtEnc; scale bar represents 2 nm. **(g)** Cutaway view of the QtEnc shell colored to local resolution and QtIMEF displayed in blue; scale bar is 2 nm. **(h)** Inner and outer diameters (through two-fold and five-fold axes) shown on a slice representation through the center of QtEnc. **(i)** Close-up through the five-fold symmetry of the QtEnc shell (grey) with an ~1 nm-sized pore. A QtIMEF density (purple) is located at a distance of ~2.5 nm to the pore **(j)** Zoomed-in view through the three-fold symmetry center with a putative pore region in its center. **(k)** Zoom-in to the two-fold symmetry center. An ~1 nm sized cleft shows two touching QtEnc monomers that seem to block the putative pore. A QtIMEF density (purple) can be found ~2.5 nm below the cleft. Scale bars in i,j,k represent 1 nm.

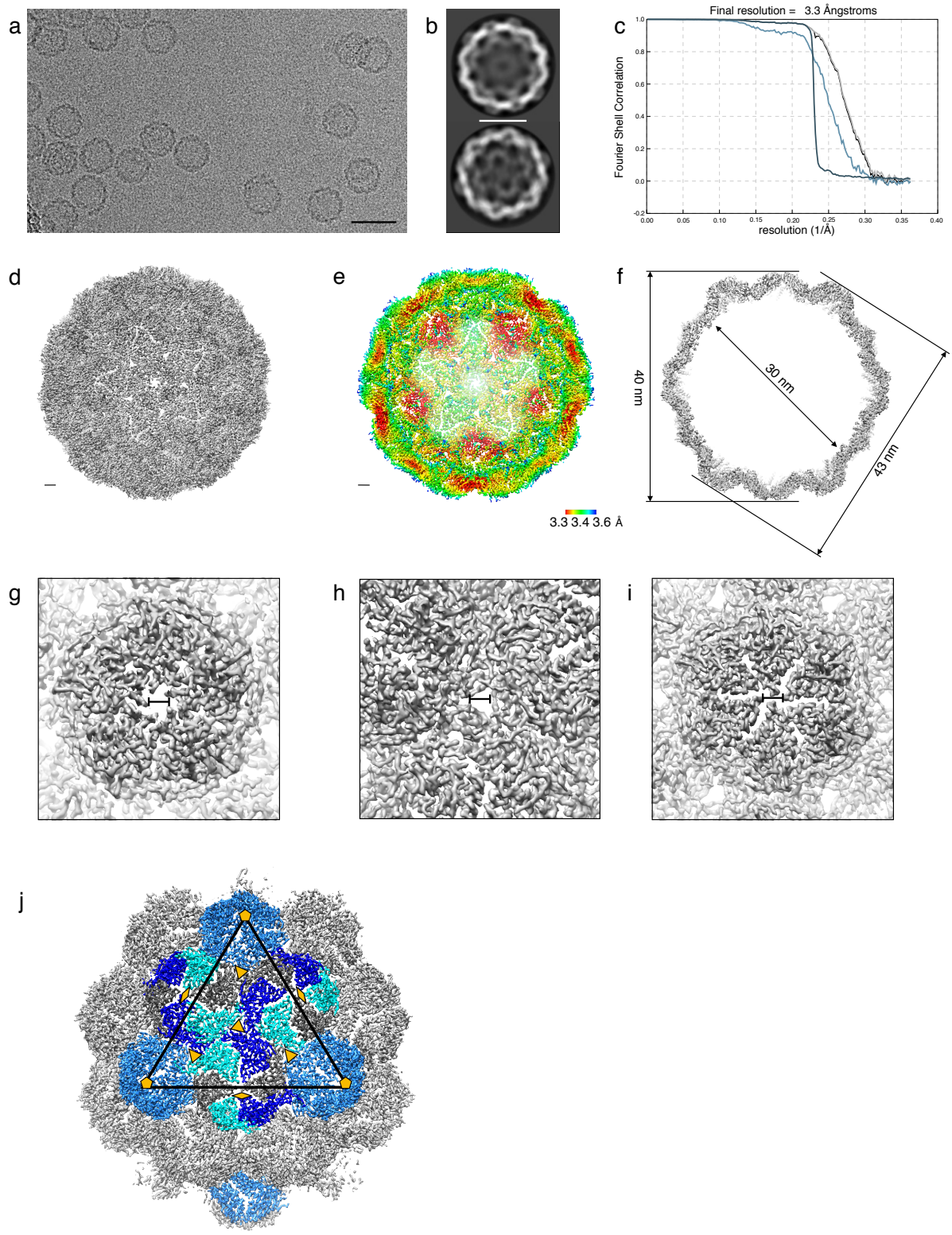

Supplementary Figure 4. Cryo-EM of QtEnc without co-expressed cargo purified from *E.coli*. **(a)** Exemplary micrograph of QtEnc nanospheres purified from *E.coli.* Scale bar represents 50 nm. **(b)** Exemplary 2D class averages of QtEnc; scale bar is 25 nm. **(c)** FSC curves of the final post-processed map showing the Fourier shell correlations of unmasked (light turquoise) and masked (light grey) maps as well as the corrected curve (black) of phase randomized, masked maps (dark turquoise). **(d)** Electrostatic potential map of QtEnc; scale bar represents 2 nm. **(e)** Cutaway view of the QtEnc shell color-coded by local resolution; scale bar is 2 nm. **(f)** Inner and outer diameters (through two-fold and five-fold axes) shown on a slice representation through the center of QtEnc. **(g)** Close-up of the five-fold symmetry center with a pore of ~1 nm in diameter. **(h)** Zoomed-in view of the three-fold symmetry center with a putative pore region in its center. **(i)** Zoom-in to the two-fold symmetry center. Scale bars in g,h,i represent 1 nm. **(j)** Surface slice of the QtEnc nanosphere showing the $T = 4$ symmetry of the capsid. Five-fold symmetry centers (light blue) are connected *via* three-fold symmetries. Symmetry centers are highlighted with orange markers (pentagon = five-fold, triangle = three-fold, diamond = two-fold). Two- and three-fold symmetry centers show individual monomer configurations (dark blue, cyan, and dark grey).

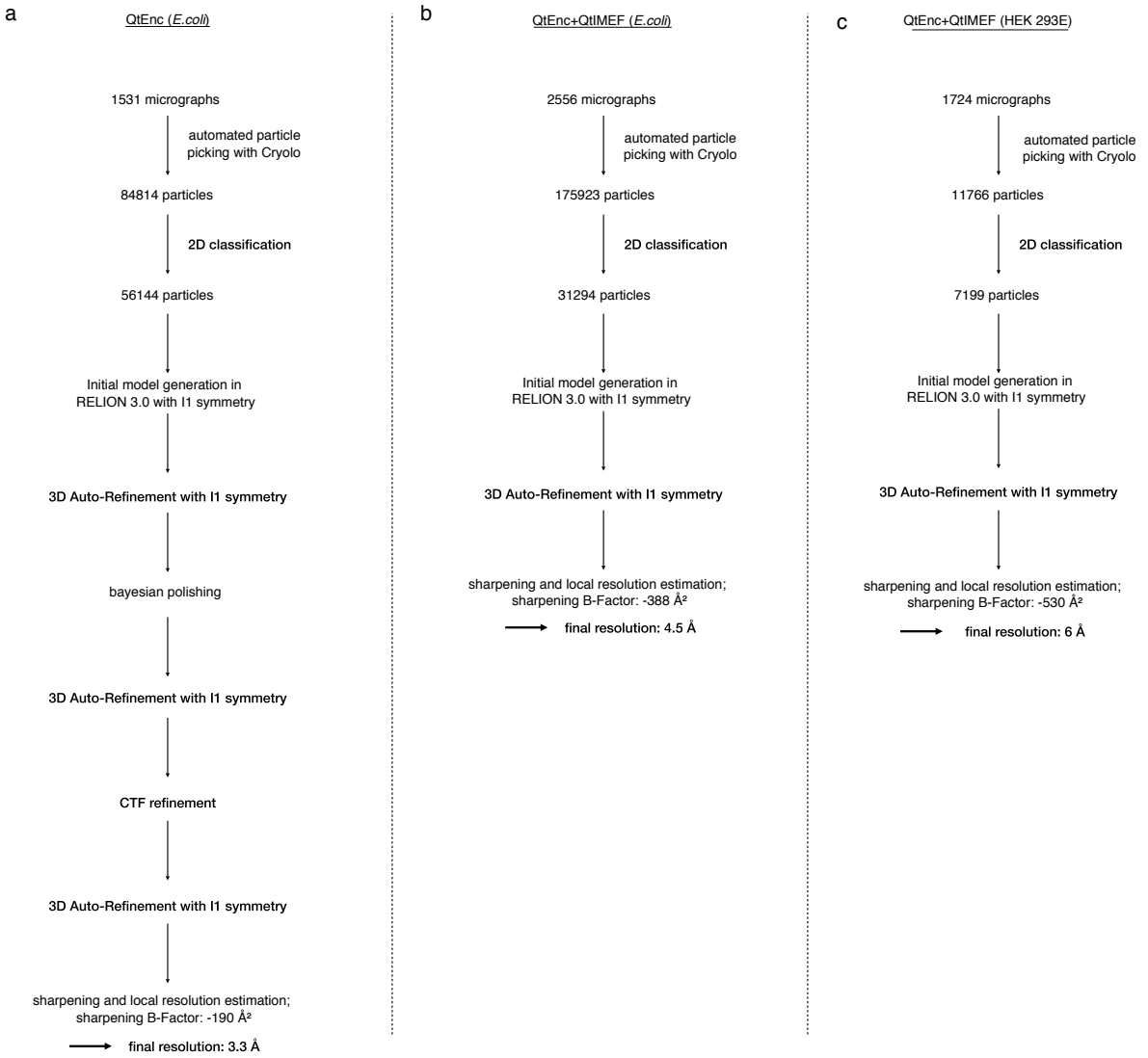

Supplementary Figure 5. Workflow diagram for cryo-EM data processing. (a) QtEnc particles without cargo expressed in *E.coli* were extracted from 1531 micrographs. Bayesian polishing and contrast transfer function (CTF) refinement were additionally applied to the dataset resulting in a final resolution of 3.3 Å. **(b)** QtEnc+QtIMEF particles expressed in *E.coli* were extracted from 2556 micrographs leading to a final resolution of 4.5 Å without Bayesian polishing and CTF refinement. **(c)** QtEnc+QtIMEF particles expressed in mammalian cells were extracted from 1724 micrographs leading to a final resolution of 6 Å without Bayesian polishing and CTF refinement.

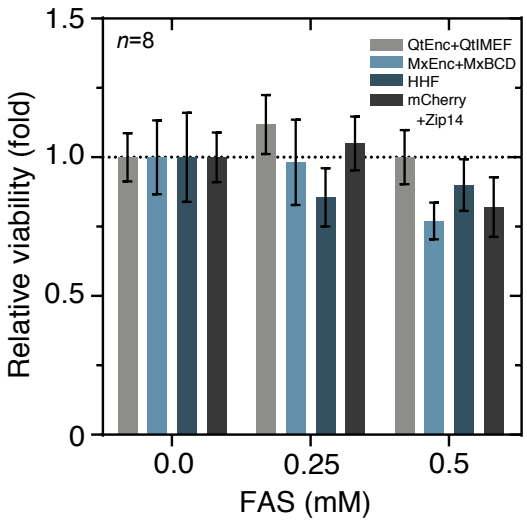

Supplementary Figure 6. Luciferase-based viability assay of HEK293T cells expressing QtEnc+QtIMEF, MxEnc+MxBCD, human H-chain ferritin (HHF) or mCherry. In all conditions, low-level Zip14 was co-expressed to boost ferrous iron uptake, which was supplemented at different concentrations (0-0.5 mM) for 36 h prior to analysis. Bars show the mean ± standard error of the mean (SEM) of n = 8 independent biological replicates. Luciferase signals were normalized to those obtained for cells without ferrous ammonium sulfate (FAS) supplementation to obtain a measure of relative viability. 2-way ANOVA did not identify significant main effects for FAS concentration (p=0.1834), gene type (p=0.4947) or interaction (p=0.7883). For a complete list of post hoc test results please see Supplementary Table 3.

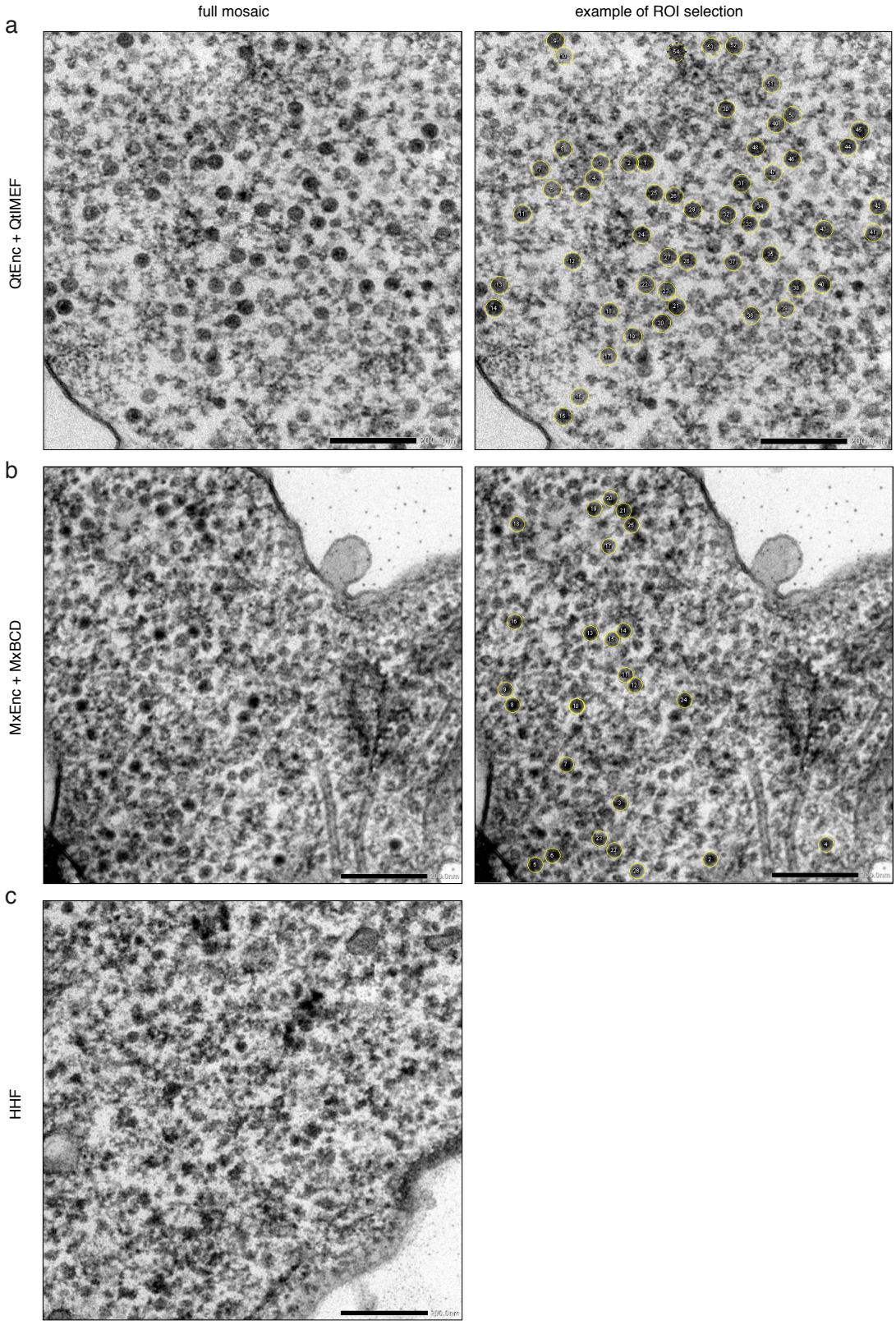

Supplementary Figure 7. Manual segmentation of intracellular encapsulins in TEM. Exemplary full frame EM image of HEK293T cells expressing **(a)** QtEnc+QtIMEF or **(b)** MxEnc+MxBCD together with low levels of Zip14. Cells were supplemented with 0.5 mM FAS for 36 h before fixation. Exemplary images on the right indicate manually segmented regions of interest (ROIs) (yellow circles) used to construct the histograms shown in Fig 4c. **(c)** Exemplary full frame EM image of HEK293T cells expressing human H-chain ferritin (HHF). ROI selection was not performed for this condition because ferritin particles could not be differentiated from ribosomes and other endogenous cellular structures. Scale bars represent 200 nm.

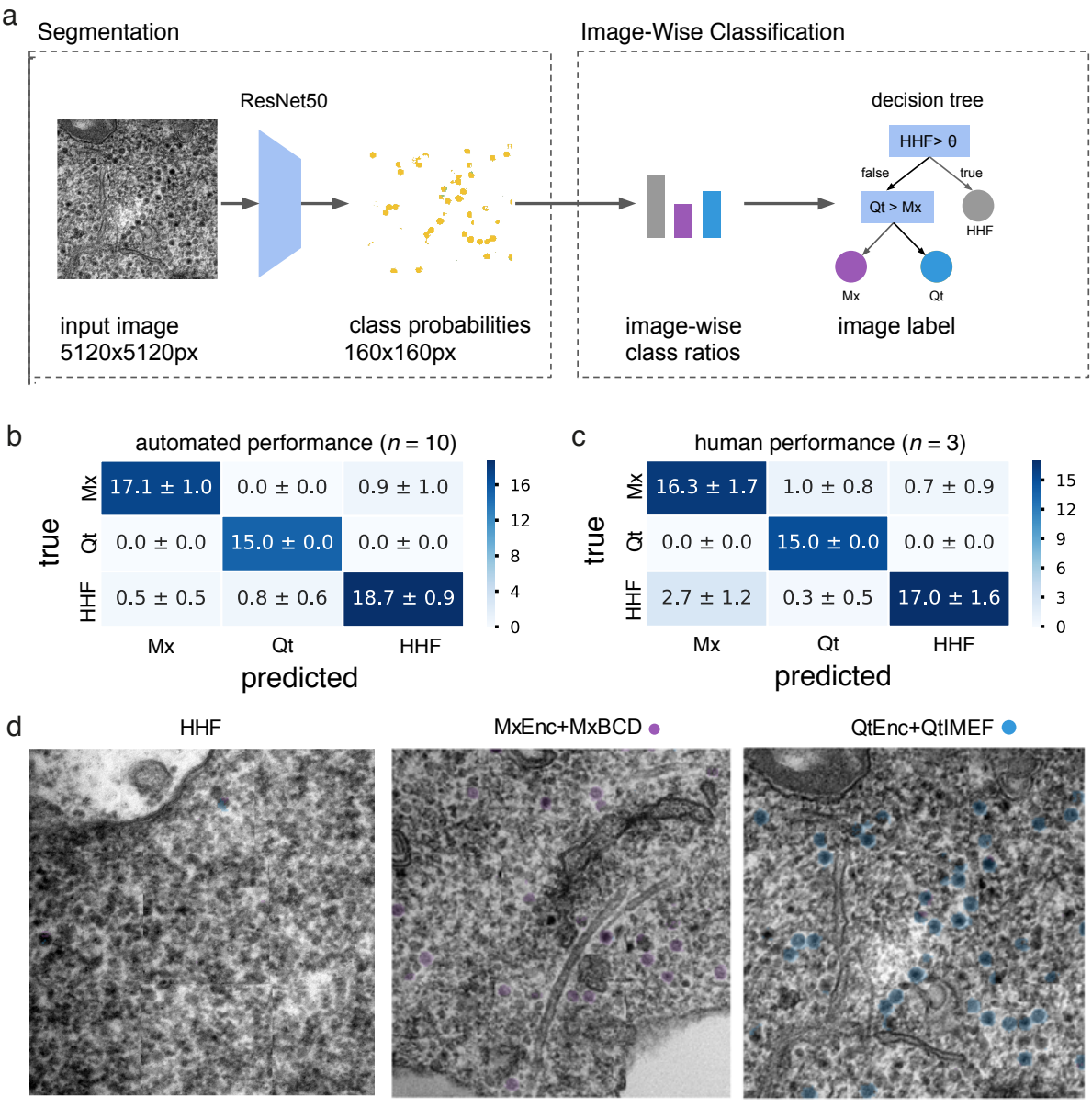

Supplementary Figure 8. Deep learning approach for classification of TEM images. (a) Deep learning approach for automated image segmentation and classification. We adapted a residual network to generate predictions at a 32x downsampled scale over spatial dimensions, allowing to locate encapsulins within each image (n = 53). To assign a label to the whole image, we computed a class histogram and determined the image label by a simple decision tree first distinguishing between background (HHF) and presence of either MxEnc+MxBCD (Mx) or QtEnc+QtIMEF (Qt) using a threshold parameter obtained with a six-fold cross-validation, followed by choosing the encapsulin type if applicable. Introduction of the threshold parameter is necessary as the majority of pixels always belongs to the background class (HHF) due to the relatively small size of encapsulins. **(b)** Confusion matrix for automated image classification. Mean and unbiased standard deviation are obtained over ten runs of the six-fold cross-validation scheme for choosing the optimal threshold parameter (with 18, 15 and 20 images for Mx/Qt/HHF respectively). **(c)** Confusion matrix showing the results of TEM image classification by human labelers (n = 3, mean and standard deviation). **(d)** Example segmentation results for control images (HHF; here with one instance of a false positive segmentation), MxEnc+MxBCD and QtEnc+QtIMEF images.

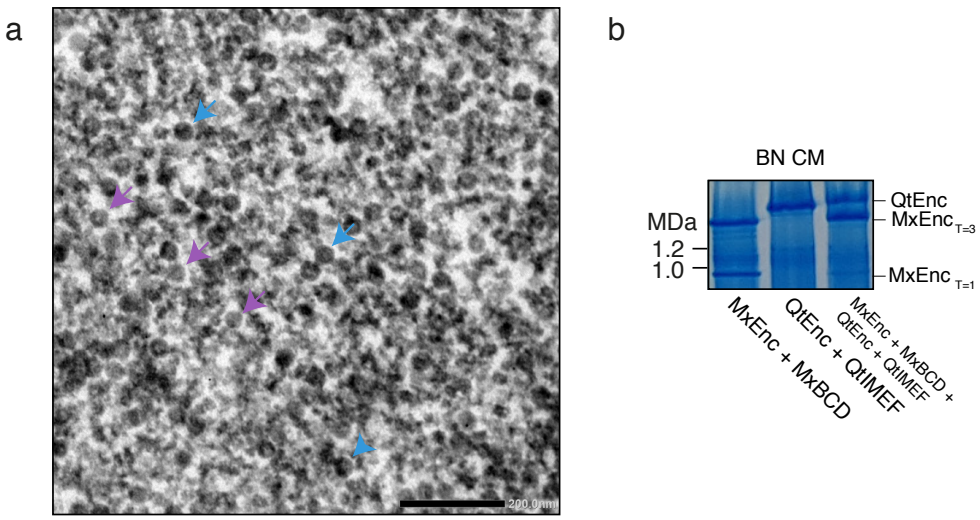

Supplementary Figure 9. TEM of HEK293T cells co-expressing Qt and Mx encapsulins. (a) TEM image of HEK293T cells expressing a mixture of MxEnc+MxBCD and QtEnc+QtIMEF. Assembled encapsulins of both sizes are apparent; purple arrows indicate Mx encapsulins (~30 nm) and blue arrows indicate Qt encapsulins (~40 nm). Scale bar represents 200 nm. **(b)** Exemplary Coomassie-stained BN-PAGE (BN CM) loaded with whole cell lysates of HEK293T expressing the gene combinations as shown in the EM image. The two distinct bands in the right lane indicate no intermixing of monomeric subunits upon co-expression of both encapsulin:cargo systems.

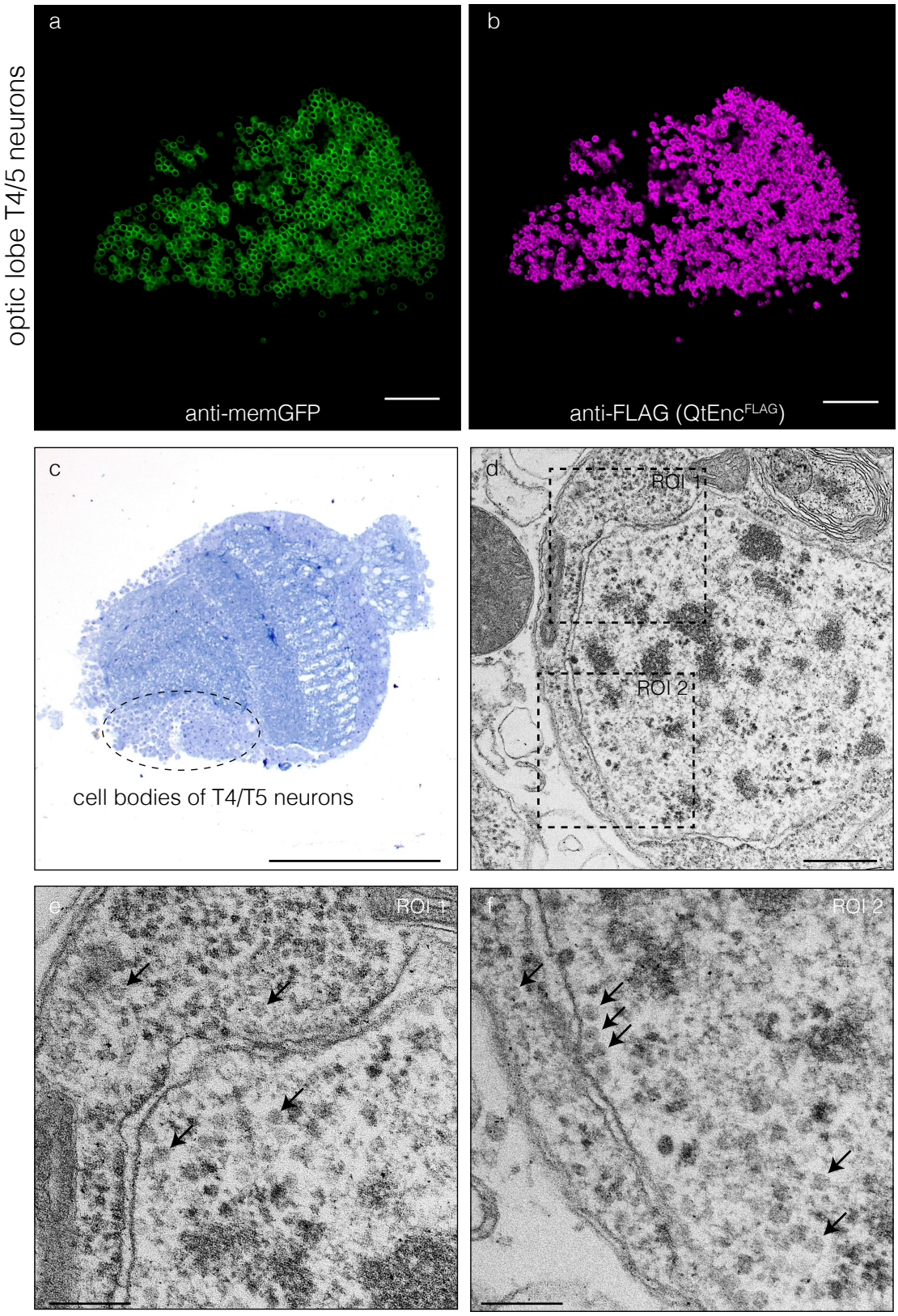

Supplementary Figure 10. *In vivo* expression of QtEnc^{FLAG}+QtIMEF in T4/T5 neurons of the *Drosophila* optic lobe. Confocal fluorescence microscopy images of dissected optic lobes showing cell bodies of T4/T5 neurons co-expressing **(a)** membrane-localized GFP (memGFP, green channel) and **(b)** FLAG-tagged QtEnc^{FLAG}+QtIMEF (anti-FLAG, magenta). Scale bars represent 20 μm. **(c)** Bright-field optical microscopy image of a semithin optic lobe section stained with toluidine blue; dashed ellipsoid indicates the cell bodies of T4/T5 neurons. Scale bar represents 100 μm. **(d-f)** TEM images of T4/T5 neuronal cell bodies from the region of interest outlined in panel c with a dashed line. **(d)** Overview image indicating the two ROIs shown in the subsequent panels, scale bar represents 500 nm. **(e-f)** ROIs 1 and 2 from panel d. The arrows point to several encapsulins in the cell cytoplasm and nucleus. Scale bar represents 200 nm.

Supplementary Table 1. Complete list of genetic constructs. Expression constructs encoding variants of the encapsulin shells and different cargo proteins are specified.

Encapsulin shell proteins		
pcDNA 3.1 (+) Zeocin MxEncA^{FLAG}	MxEncA-GSG-DYKDDDDK*	UniProt: EncA: MXAN_3556
pcDNA 3.1 (+) Zeocin QtEnc^{FLAG}	QtEnc-GSG-DYKDDDDK*	WP_039238471.1, UniProt: A0A0F5HPP7_9BACI
pcDNA 3.1 (+) Zeocin QtEnc^{Farn}	QtEnc-GSG-GCMSCKCVLS*	WP_039238471.1, UniProt: A0A0F5HPP7_9BACI
pRSFDuet-1 QtEnc$^{Strep\text{-}Tag\ II}$	QtEnc-GSG-WSHPQFEK*	WP_039238471.1, UniProt: A0A0F5HPP7_9BACI
pDSG-IBAwt2 BM40-QtEnc$^{Strep\text{-}Tag\ II}$	MRAWIFFLLCLAGRALAA-QtEnc-GSGSA-WSHPQFEK*	WP_039238471.1, UniProt: A0A0F5HPP7_9BACI
Encapsulin cargo proteins		
pcDNA 3.1 (+) Zeocin MxEncBCD$_{P2A}$	MxEncB-GSG-ATNFSLLKQAGDVEENPGP-MxEncC-GSG-ATNFSLLKQAGDVEENPGP-MxEncD*	UniProt: EncB: MXAN_3557, EncC: MXAN_4464, EncD: MXAN_2410
pcDNA 3.1 (+) Zeocin QtIMEF	QtIMEF*	WP_039238473.1, UniProt: A0A0F5HNH9_9BACI
pRSFDuet-1 QtEnc$^{Strep\text{-}Tag\ II}$+QtIMEF	MCS1: QtIMEF* MCS2: QtEnc-GSG-WSHPQFEK*	UniProt: QtEnc: A0A0F5HPP7_9BACI, QtIMEF: A0A0F5HNH9_9BACI
pDSG-IBAwt2 BM40-QtIMEF	MRAWIFFLLCLAGRALAA-QtIMEF*	WP_039238473.1, UniProt: A0A0F5HNH9_9BACI
Encapsulin constructs for transgenic fly generation		
pJFRC7-20XUAS-IVS-QtIMEF$_{P2A}$QtEnc^{FLAG}-IRES2-mScarlet-I	QtIMEF-GSG-ATNFSLLKQAGDVEENPGP-QtEnc-GSG-DYKDDDDK*-IRES2-mScarlet-I	UniProt: QtEnc: A0A0F5HPP7_9BACI, QtIMEF: A0A0F5HNH9_9BACI mScarlet-I: https://www.addgene.org/104007/
Other proteins		
pcDNA 3.1 (+) MmZip14-FLAG	MmZip14-GGGGGSGGGGS-DYKDDDDK*	UniProt: Q75N73
pcDNA 3.1 (+) HHF	HHF*	UniProt: P02794

Supplementary Table 2. Properties of the two encapsulin systems.

	MxEnc	QtEnc
Symmetry of icosahedral shell	$T = 1$ and $T = 3$	$T = 4$
Number of subunits	60 ($T = 1$), 180 ($T = 3$)	240 ($T = 4$)
Molecular weight of monomers (kDa) [1]	MxEnc: 33; MxB: 17; MxC: 13; MxD: 11	QtEnc: 32; QtIMEF: 23
Number of cargo proteins per shell [2]	86 ± 3 (MxB), 93 ± 9 (MxC), 50 ± 15 (MxD)	231 ± 5 (QtIMEF)
Shell outer diameter of cargo loaded compartment (nm) [3]	~32	~43
Iron atoms per protein shell [4]	18856 ± 807	35097 ± 853

[1] MxEnc: taken from supplementary reference[1], QtEnc: taken from supplementary reference[2]
[2] calculated from densitometric SDS-PAGE analysis from $n = 3$ independent samples
[3] values for MxEnc ($T = 3$ assembly) were determined using single particle cryoEM[1,3]
[4] measured by ICP-MS ($n = 2$)

Supplementary Table 3. Results of the post hoc tests.

Iron loading in mammalian cells without Zip14 (Figure 3c)				
0:MxEnc+MxBCD vs. 0:QtEnc+IMEF	Two-way ANOVA, Bonferroni-correction	> 0.9999	ns	n =3
0:MxEnc+MxBCD vs. 0.125:MxEnc+MxBCD	Two-way ANOVA, Bonferroni-correction	> 0.9999	ns	n =3
0:MxEnc+MxBCD vs. 0.125:QtEnc+IMEF	Two-way ANOVA, Bonferroni-correction	> 0.9999	ns	n =3
0:MxEnc+MxBCD vs. 0.25:MxEnc+MxBCD	Two-way ANOVA, Bonferroni-correction	> 0.9999	ns	n =3
0:MxEnc+MxBCD vs. 0.25:QtEnc+IMEF	Two-way ANOVA, Bonferroni-correction	> 0.9999	ns	n =3
0:MxEnc+MxBCD vs. 0.50:MxEnc+MxBCD	Two-way ANOVA, Bonferroni-correction	0.5833	ns	n =3
0:MxEnc+MxBCD vs. 0.50:QtEnc+IMEF	Two-way ANOVA, Bonferroni-correction	0.0001	***	n =3
0:MxEnc+MxBCD vs. 1:MxEnc+MxBCD	Two-way ANOVA, Bonferroni-correction	0.0036	**	n =3
0:MxEnc+MxBCD vs. 1:QtEnc+IMEF	Two-way ANOVA, Bonferroni-correction	< 0.0001	****	n =3
0:QtEnc+IMEF vs. 0.125:MxEnc+MxBCD	Two-way ANOVA, Bonferroni-correction	> 0.9999	ns	n =3
0:QtEnc+IMEF vs. 0.125:QtEnc+IMEF	Two-way ANOVA, Bonferroni-correction	> 0.9999	ns	n =3
0:QtEnc+IMEF vs. 0.25:MxEnc+MxBCD	Two-way ANOVA, Bonferroni-correction	> 0.9999	ns	n =3
0:QtEnc+IMEF vs. 0.25:QtEnc+IMEF	Two-way ANOVA, Bonferroni-correction	> 0.9999	ns	n =3
0:QtEnc+IMEF vs. 0.50:MxEnc+MxBCD	Two-way ANOVA, Bonferroni-correction	> 0.9999	ns	n =3
0:QtEnc+IMEF vs. 0.50:QtEnc+IMEF	Two-way ANOVA, Bonferroni-correction	0.0166	*	n =3
0:QtEnc+IMEF vs. 1:MxEnc+MxBCD	Two-way ANOVA, Bonferroni-correction	0.4837	ns	n =3
0:QtEnc+IMEF vs. 1:QtEnc+IMEF	Two-way ANOVA, Bonferroni-correction	< 0.0001	****	n =3
0.125:MxEnc+MxBCD vs. 0.125:QtEnc+IMEF	Two-way ANOVA, Bonferroni-correction	> 0.9999	ns	n =3
0.125:MxEnc+MxBCD vs. 0.25:MxEnc+MxBCD	Two-way ANOVA, Bonferroni-correction	> 0.9999	ns	n =3
0.125:MxEnc+MxBCD vs. 0.25:QtEnc+IMEF	Two-way ANOVA, Bonferroni-correction	> 0.9999	ns	n =3
0.125:MxEnc+MxBCD vs. 0.50:MxEnc+MxBCD	Two-way ANOVA, Bonferroni-correction	> 0.9999	ns	n =3
0.125:MxEnc+MxBCD vs. 0.50:QtEnc+IMEF	Two-way ANOVA, Bonferroni-correction	0.0427	*	n =3

0.125:MxEnc+MxBCD vs. 1:MxEnc+MxBCD	Two-way ANOVA, Bonferroni-correction	0.8393	ns	n =3
0.125:MxEnc+MxBCD vs. 1:QtEnc+IMEF	Two-way ANOVA, Bonferroni-correction	< 0.0001	****	n =3
0.125:QtEnc+IMEF vs. 0.25:MxEnc+MxBCD	Two-way ANOVA, Bonferroni-correction	> 0.9999	ns	n =3
0.125:QtEnc+IMEF vs. 0.25:QtEnc+IMEF	Two-way ANOVA, Bonferroni-correction	> 0.9999	ns	n =3
0.125:QtEnc+IMEF vs. 0.50:MxEnc+MxBCD	Two-way ANOVA, Bonferroni-correction	> 0.9999	ns	n =3
0.125:QtEnc+IMEF vs. 0.50:QtEnc+IMEF	Two-way ANOVA, Bonferroni-correction	0.0012	**	n =3
0.125:QtEnc+IMEF vs. 1:MxEnc+MxBCD	Two-way ANOVA, Bonferroni-correction	0.0347	*	n =3
0.125:QtEnc+IMEF vs. 1:QtEnc+IMEF	Two-way ANOVA, Bonferroni-correction	< 0.0001	****	n =3
0.25:MxEnc+MxBCD vs. 0.25:QtEnc+IMEF	Two-way ANOVA, Bonferroni-correction	> 0.9999	ns	n =3
0.25:MxEnc+MxBCD vs. 0.50:MxEnc+MxBCD	Two-way ANOVA, Bonferroni-correction	> 0.9999	ns	n =3
0.25:MxEnc+MxBCD vs. 0.50:QtEnc+IMEF	Two-way ANOVA, Bonferroni-correction	0.0073	**	n =3
0.25:MxEnc+MxBCD vs. 1:MxEnc+MxBCD	Two-way ANOVA, Bonferroni-correction	0.2175	ns	n =3
0.25:MxEnc+MxBCD vs. 1:QtEnc+IMEF	Two-way ANOVA, Bonferroni-correction	< 0.0001	****	n =3
0.25:QtEnc+IMEF vs. 0.50:MxEnc+MxBCD	Two-way ANOVA, Bonferroni-correction	> 0.9999	ns	n =3
0.25:QtEnc+IMEF vs. 0.50:QtEnc+IMEF	Two-way ANOVA, Bonferroni-correction	0.0249	*	n =3
0.25:QtEnc+IMEF vs. 1:MxEnc+MxBCD	Two-way ANOVA, Bonferroni-correction	0.7104	ns	n =3
0.25:QtEnc+IMEF vs. 1:QtEnc+IMEF	Two-way ANOVA, Bonferroni-correction	< 0.0001	****	n =3
0.50:MxEnc+MxBCD vs. 0.50:QtEnc+IMEF	Two-way ANOVA, Bonferroni-correction	0.0618	ns	n =3
0.50:MxEnc+MxBCD vs. 1:MxEnc+MxBCD	Two-way ANOVA, Bonferroni-correction	> 0.,9999	ns	n =3
0.50:MxEnc+MxBCD vs. 1:QtEnc+IMEF	Two-way ANOVA, Bonferroni-correction	< 0.0001	****	n =3
0.50:QtEnc+IMEF vs. 1:MxEnc+MxBCD	Two-way ANOVA, Bonferroni-correction	>0.9999	ns	n =3
0.50:QtEnc+IMEF vs. 1:QtEnc+IMEF	Two-way ANOVA, Bonferroni-correction	< 0.0001	****	n =3
1:MxEnc+MxBCD vs. 1:QtEnc+IMEF	Two-way ANOVA, Bonferroni-correction	< 0.0001	****	n =3
Iron loading in mammalian cells with Zip14 (Figure 3c)				

0:MxEnc+MxBCD vs. 0:QtEnc+IMEF	Two-way ANOVA, Bonferroni-correction	> 0.9999	ns	n =3
0:MxEnc+MxBCD vs. 0.125:MxEnc+MxBCD	Two-way ANOVA, Bonferroni-correction	> 0.9999	ns	n =3
0:MxEnc+MxBCD vs. 0.125:QtEnc+IMEF	Two-way ANOVA, Bonferroni-correction	0.1028	ns	n =3
0:MxEnc+MxBCD vs. 0.25:MxEnc+MxBCD	Two-way ANOVA, Bonferroni-correction	0.0105	*	n =3
0:MxEnc+MxBCD vs. 0.25:QtEnc+IMEF	Two-way ANOVA, Bonferroni-correction	<0.0001	****	n =3
0:MxEnc+MxBCD vs. 0.50:MxEnc+MxBCD	Two-way ANOVA, Bonferroni-correction	<0.0001	****	n =3
0:MxEnc+MxBCD vs. 0.50:QtEnc+IMEF	Two-way ANOVA, Bonferroni-correction	< 0.0001	****	n =3
0:MxEnc+MxBCD vs. 1:MxEnc+MxBCD	Two-way ANOVA, Bonferroni-correction	< 0.0001	****	n =3
0:MxEnc+MxBCD vs. 1:QtEnc+IMEF	Two-way ANOVA, Bonferroni-correction	< 0.0001	****	n =3
0:QtEnc+IMEF vs. 0.125:MxEnc+MxBCD	Two-way ANOVA, Bonferroni-correction	> 0.9999	ns	n =3
0:QtEnc+IMEF vs. 0.125:QtEnc+IMEF	Two-way ANOVA, Bonferroni-correction	0.7190	ns	n =3
0:QtEnc+IMEF vs. 0.25:MxEnc+MxBCD	Two-way ANOVA, Bonferroni-correction	0.0784	ns	n =3
0:QtEnc+IMEF vs. 0.25:QtEnc+IMEF	Two-way ANOVA, Bonferroni-correction	< 0.0001	****	n =3
0:QtEnc+IMEF vs. 0.50:MxEnc+MxBCD	Two-way ANOVA, Bonferroni-correction	0.0001	***	n =3
0:QtEnc+IMEF vs. 0.50:QtEnc+IMEF	Two-way ANOVA, Bonferroni-correction	< 0.0001	****	n =3
0:QtEnc+IMEF vs. 1:MxEnc+MxBCD	Two-way ANOVA, Bonferroni-correction	< 0.0001	****	n =3
0:QtEnc+IMEF vs. 1:QtEnc+IMEF	Two-way ANOVA, Bonferroni-correction	< 0.0001	****	n =3
0.125:MxEnc+MxBCD vs. 0.125:QtEnc+IMEF	Two-way ANOVA, Bonferroni-correction	> 0.9999	ns	n =3
0.125:MxEnc+MxBCD vs. 0.25:MxEnc+MxBCD	Two-way ANOVA, Bonferroni-correction	0.1767	ns	n =3
0.125:MxEnc+MxBCD vs. 0.25:QtEnc+IMEF	Two-way ANOVA, Bonferroni-correction	0.0002	***	n =3
0.125:MxEnc+MxBCD vs. 0.50:MxEnc+MxBCD	Two-way ANOVA, Bonferroni-correction	0.0003	***	n =3
0.125:MxEnc+MxBCD vs. 0.50:QtEnc+IMEF	Two-way ANOVA, Bonferroni-correction	< 0.0001	****	n =3
0.125:MxEnc+MxBCD vs. 1:MxEnc+MxBCD	Two-way ANOVA, Bonferroni-correction	< 0.0001	****	n =3
0.125:MxEnc+MxBCD vs. 1:QtEnc+IMEF	Two-way ANOVA, Bonferroni-correction	< 0.0001	****	n =3

0.125:QtEnc+IMEF vs. 0.25:MxEnc+MxBCD	Two-way ANOVA, Bonferroni-correction	> 0.9999	ns	n =3
0.125:QtEnc+IMEF vs. 0.25:QtEnc+IMEF	Two-way ANOVA, Bonferroni-correction	0.0272	*	n =3
0.125:QtEnc+IMEF vs. 0.50:MxEnc+MxBCD	Two-way ANOVA, Bonferroni-correction	0.0540	ns	n =3
0.125:QtEnc+IMEF vs. 0.50:QtEnc+IMEF	Two-way ANOVA, Bonferroni-correction	< 0.0001	****	n =3
0.125:QtEnc+IMEF vs. 1:MxEnc+MxBCD	Two-way ANOVA, Bonferroni-correction	< 0.0001	****	n =3
0.125:QtEnc+IMEF vs. 1:QtEnc+IMEF	Two-way ANOVA, Bonferroni-correction	< 0.0001	****	n =3
0.25:MxEnc+MxBCD vs. 0.25:QtEnc+IMEF	Two-way ANOVA, Bonferroni-correction	0.2626	ns	n =3
0.25:MxEnc+MxBCD vs. 0.50:MxEnc+MxBCD	Two-way ANOVA, Bonferroni-correction	0.5066	ns	n =3
0.25:MxEnc+MxBCD vs. 0.50:QtEnc+IMEF	Two-way ANOVA, Bonferroni-correction	< 0.0001	****	n =3
0.25:MxEnc+MxBCD vs. 1:MxEnc+MxBCD	Two-way ANOVA, Bonferroni-correction	< 0.0001	****	n =3
0.25:MxEnc+MxBCD vs. 1:QtEnc+IMEF	Two-way ANOVA, Bonferroni-correction	< 0.0001	****	n =3
0.25:QtEnc+IMEF vs. 0.50:MxEnc+MxBCD	Two-way ANOVA, Bonferroni-correction	>0.9999	ns	n =3
0.25:QtEnc+IMEF vs. 0.50:QtEnc+IMEF	Two-way ANOVA, Bonferroni-correction	0.0095	**	n =3
0.25:QtEnc+IMEF vs. 1:MxEnc+MxBCD	Two-way ANOVA, Bonferroni-correction	<0.0001	****	n =3
0.25:QtEnc+IMEF vs. 1:QtEnc+IMEF	Two-way ANOVA, Bonferroni-correction	< 0.0001	****	n =3
0.50:MxEnc+MxBCD vs. 0.50:QtEnc+IMEF	Two-way ANOVA, Bonferroni-correction	0.0048	**	n =3
0.50:MxEnc+MxBCD vs. 1:MxEnc+MxBCD	Two-way ANOVA, Bonferroni-correction	< 0.0001	****	n =3
0.50:MxEnc+MxBCD vs. 1:QtEnc+IMEF	Two-way ANOVA, Bonferroni-correction	< 0.0001	****	n =3
0.50:QtEnc+IMEF vs. 1:MxEnc+MxBCD	Two-way ANOVA, Bonferroni-correction	0.0017	**	n =3
0.50:QtEnc+IMEF vs. 1:QtEnc+IMEF	Two-way ANOVA, Bonferroni-correction	0.0001	***	n =3
1:MxEnc+MxBCD vs. 1:QtEnc+IMEF	Two-way ANOVA, Bonferroni-correction	> 0.9999	ns	n =3
Viability assay (Supplementary Figure 6)				
0.00:mCherry vs. 0.00:HHF	Two-way ANOVA, Bonferroni-correction	p > 0.9999	ns	n = 8
0.00:mCherry vs. 0.00:Mx	Two-way ANOVA, Bonferroni-correction	p > 0.9999	ns	n = 8

0.00:mCherry vs. 0.00:QtEnc	Two-way ANOVA, Bonferroni-correction	p > 0.9999	ns	n = 8
0.00:mCherry vs. 0.25:mCherry	Two-way ANOVA, Bonferroni-correction	p > 0.9999	ns	n = 8
0.00:mCherry vs. 0.25:HHF	Two-way ANOVA, Bonferroni-correction	p > 0.9999	ns	n = 8
0.00:mCherry vs. 0.25:Mx	Two-way ANOVA, Bonferroni-correction	p > 0.9999	ns	n = 8
0.00:mCherry vs. 0.25:QtEnc	Two-way ANOVA, Bonferroni-correction	p > 0.9999	ns	n = 8
0.00:mCherry vs. 0.50:mCherry	Two-way ANOVA, Bonferroni-correction	p > 0.9999	ns	n = 8
0.00:mCherry vs. 0.50:HHF	Two-way ANOVA, Bonferroni-correction	p > 0.9999	ns	n = 8
0.00:mCherry vs. 0.50:Mx	Two-way ANOVA, Bonferroni-correction	p > 0.9999	ns	n = 8
0.00:mCherry vs. 0.50:QtEnc	Two-way ANOVA, Bonferroni-correction	p > 0.9999	ns	n = 8
0.00:HHF vs. 0.00:Mx	Two-way ANOVA, Bonferroni-correction	p > 0.9999	ns	n = 8
0.00:HHF vs. 0.00:QtEnc	Two-way ANOVA, Bonferroni-correction	p > 0.9999	ns	n = 8
0.00:HHF vs. 0.25:mCherry	Two-way ANOVA, Bonferroni-correction	p > 0.9999	ns	n = 8
0.00:HHF vs. 0.25:HHF	Two-way ANOVA, Bonferroni-correction	p > 0.9999	ns	n = 8
0.00:HHF vs. 0.25:Mx	Two-way ANOVA, Bonferroni-correction	p > 0.9999	ns	n = 8
0.00:HHF vs. 0.25:QtEnc	Two-way ANOVA, Bonferroni-correction	p > 0.9999	ns	n = 8
0.00:HHF vs. 0.50:mCherry	Two-way ANOVA, Bonferroni-correction	p > 0.9999	ns	n = 8
0.00:HHF vs. 0.50:HHF	Two-way ANOVA, Bonferroni-correction	p > 0.9999	ns	n = 8
0.00:HHF vs. 0.50:Mx	Two-way ANOVA, Bonferroni-correction	p > 0.9999	ns	n = 8
0.00:HHF vs. 0.50:QtEnc	Two-way ANOVA, Bonferroni-correction	p > 0.9999	ns	n = 8
0.00:Mx vs. 0.00:QtEnc	Two-way ANOVA, Bonferroni-correction	p > 0.9999	ns	n = 8
0.00:Mx vs. 0.25:mCherry	Two-way ANOVA, Bonferroni-correction	p > 0.9999	ns	n = 8
0.00:Mx vs. 0.25:HHF	Two-way ANOVA, Bonferroni-correction	p > 0.9999	ns	n = 8
0.00:Mx vs. 0.25:Mx	Two-way ANOVA, Bonferroni-correction	p > 0.9999	ns	n = 8
0.00:Mx vs. 0.25:QtEnc	Two-way ANOVA, Bonferroni-correction	p > 0.9999	ns	n = 8

0.00:Mx vs. 0.50:mCherry	Two-way ANOVA, Bonferroni-correction	p > 0.9999	ns	n = 8
0.00:Mx vs. 0.50:HHF	Two-way ANOVA, Bonferroni-correction	p > 0.9999	ns	n = 8
0.00:Mx vs. 0.50:Mx	Two-way ANOVA, Bonferroni-correction	p > 0.9999	ns	n = 8
0.00:Mx vs. 0.50:QtEnc	Two-way ANOVA, Bonferroni-correction	p = 0.1396	ns	n = 8
0.00:QtEnc vs. 0.25:mCherry	Two-way ANOVA, Bonferroni-correction	p > 0.9999	ns	n = 8
0.00:QtEnc vs. 0.25:HHF	Two-way ANOVA, Bonferroni-correction	p > 0.9999	ns	n = 8
0.00:QtEnc vs. 0.25:Mx	Two-way ANOVA, Bonferroni-correction	p > 0.9999	ns	n = 8
0.00:QtEnc vs. 0.25:QtEnc	Two-way ANOVA, Bonferroni-correction	p > 0.9999	ns	n = 8
0.00:QtEnc vs. 0.50:mCherry	Two-way ANOVA, Bonferroni-correction	p > 0.9999	ns	n = 8
0.00:QtEnc vs. 0.50:HHF	Two-way ANOVA, Bonferroni-correction	p > 0.9999	ns	n = 8
0.00:QtEnc vs. 0.50:Mx	Two-way ANOVA, Bonferroni-correction	p > 0.9999	ns	n = 8
0.00:QtEnc vs. 0.50:QtEnc	Two-way ANOVA, Bonferroni-correction	p > 0.9999	ns	n = 8
0.25:mCherry vs. 0.25:HHF	Two-way ANOVA, Bonferroni-correction	p > 0.9999	ns	n = 8
0.25:mCherry vs. 0.25:Mx	Two-way ANOVA, Bonferroni-correction	p > 0.9999	ns	n = 8
0.25:mCherry vs. 0.25:QtEnc	Two-way ANOVA, Bonferroni-correction	p > 0.9999	ns	n = 8
0.25:mCherry vs. 0.50:mCherry	Two-way ANOVA, Bonferroni-correction	p > 0.9999	ns	n = 8
0.25:mCherry vs. 0.50:HHF	Two-way ANOVA, Bonferroni-correction	p > 0.9999	ns	n = 8
0.25:mCherry vs. 0.50:Mx	Two-way ANOVA, Bonferroni-correction	p > 0.9999	ns	n = 8
0.25:mCherry vs. 0.50:QtEnc	Two-way ANOVA, Bonferroni-correction	p > 0.9999	ns	n = 8
0.25:HHF vs. 0.25:Mx	Two-way ANOVA, Bonferroni-correction	p > 0.9999	ns	n = 8
0.25:HHF vs. 0.25:QtEnc	Two-way ANOVA, Bonferroni-correction	p > 0.9999	ns	n = 8
0.25:HHF vs. 0.50:mCherry	Two-way ANOVA, Bonferroni-correction	p > 0.9999	ns	n = 8
0.25:HHF vs. 0.50:HHF	Two-way ANOVA, Bonferroni-correction	p > 0.9999	ns	n = 8
0.25:HHF vs. 0.50:Mx	Two-way ANOVA, Bonferroni-correction	p > 0.9999	ns	n = 8

0.25:HHF vs. 0.50:QtEnc	Two-way ANOVA, Bonferroni-correction	p > 0.9999	ns	n = 8
0.25:Mx vs. 0.25:QtEnc	Two-way ANOVA, Bonferroni-correction	p > 0.9999	ns	n = 8
0.25:Mx vs. 0.50:mCherry	Two-way ANOVA, Bonferroni-correction	p > 0.9999	ns	n = 8
0.25:Mx vs. 0.50:HHF	Two-way ANOVA, Bonferroni-correction	p > 0.9999	ns	n = 8
0.25:Mx vs. 0.50:Mx	Two-way ANOVA, Bonferroni-correction	p > 0.9999	ns	n = 8
0.25:Mx vs. 0.50:QtEnc	Two-way ANOVA, Bonferroni-correction	p > 0.9999	ns	n = 8
0.25:QtEnc vs. 0.50:mCherry	Two-way ANOVA, Bonferroni-correction	p > 0.9999	ns	n = 8
0.25:QtEnc vs. 0.50:HHF	Two-way ANOVA, Bonferroni-correction	p > 0.9999	ns	n = 8
0.25:QtEnc vs. 0.50:Mx	Two-way ANOVA, Bonferroni-correction	p > 0.9999	ns	n = 8
0.25:QtEnc vs. 0.50:QtEnc	Two-way ANOVA, Bonferroni-correction	p > 0.9999	ns	n = 8
0.50:mCherry vs. 0.50:HHF	Two-way ANOVA, Bonferroni-correction	p > 0.9999	ns	n = 8
0.50:mCherry vs. 0.50:Mx	Two-way ANOVA, Bonferroni-correction	p > 0.9999	ns	n = 8
0.50:mCherry vs. 0.50:QtEnc	Two-way ANOVA, Bonferroni-correction	p > 0.9999	ns	n = 8
0.50:HHF vs. 0.50:Mx	Two-way ANOVA, Bonferroni-correction	p > 0.9999	ns	n = 8
0.50:HHF vs. 0.50:QtEnc	Two-way ANOVA, Bonferroni-correction	p > 0.9999	ns	n = 8
0.50:Mx vs. 0.50:QtEnc	Two-way ANOVA, Bonferroni-correction	p > 0.9999	ns	n = 8

SUPPLEMENTARY REFERENCES

(1) McHugh, C. A.; Fontana, J.; Nemecek, D.; Cheng, N.; Aksyuk, A. A.; Heymann, J. B.; Winkler, D. C.; Lam, A. S.; Wall, J. S.; Steven, A. C.; Others. A Virus Capsid-like Nanocompartment That Stores Iron and Protects Bacteria from Oxidative Stress. *EMBO J.* **2014**, *33*, 1896–1911.

(2) Giessen, T. W.; Silver, P. A. Widespread Distribution of Encapsulin Nanocompartments Reveals Functional Diversity. *Nat Microbiol* **2017**, *2*, 17029.

(3) Sigmund, F.; Massner, C.; Erdmann, P.; Stelzl, A.; Rolbieski, H.; Desai, M.; Bricault, S.; Wörner, T. P.; Snijder, J.; Geerlof, A.; Fuchs, H.; Hrabě de Angelis, M.; Heck, A. J. R.; Jasanoff, A.; Ntziachristos, V.; Plitzko, J.; Westmeyer, G. G. Bacterial Encapsulins as Orthogonal Compartments for Mammalian Cell Engineering. *Nat. Commun.* **2018**, *9*, 1990.